JOURNAL OF COLLOID AND INTERFACE SCIENCE **201,** 210–219 (1998)
ARTICLE NO. CS985399

Studies of Surface Properties of Disperse Silica and Alumina by Luminescence Measurements and Nitrogen Adsorption

Yu. D. Glinka,* C. P. Jaroniec,† and M. Jaroniec‡,[1]

*Institute of Surface Chemistry of the National Academy of Sciences of Ukraine, Prospekt Nauki 31, Kiev 252650, Ukraine;
†Department of Chemistry, Massachusetts Institute of Technology, Cambridge, Massachusetts 02139; and
‡Separation and Surface Science Center, Department of Chemistry, Kent State University, Kent, Ohio 44242

Received September 17, 1997; accepted December 30, 1997

A new method for the determination of the adsorption energy distribution of water molecules on disperse silica and alumina surfaces is presented. This method takes into account interactions between the surface and hydrated uranyl (UO_2^{2+}) groups, which are luminescent probes. Changes in the spectroscopic characteristics of uranyl ions, measured under selective laser excitation, have been used to evaluate the adsorption activity of different surface sites. The adsorption energy distributions of water molecules, which coordinate the UO_2^{2+} ions in the equatorial plane, were evaluated for disperse inorganic oxides on the basis of luminescence measurements and were compared with the energy distribution curves calculated from nitrogen adsorption at 77.35 K, which is the standard technique for the characterization of porous materials. In addition, high-resolution thermogravimetric measurements were performed to supplement information about surface properties of the materials studied. The differences in the nature of adsorption interactions for nitrogen and water probe molecules are discussed in context of their impact on the shape of the resulting adsorption energy distributions. The low-energy and high-energy parts of these distributions were attributed to the physically and chemically adsorbed water molecules, respectively. © 1998 Academic Press

Key Words: **luminescence spectra; adsorption energy; UO_2^{2+} ions; hydrated uranyl groups; silica surface; alumina surface; nitrogen adsorption; thermogravimetric measurements; adsorption energy distribution.**

INTRODUCTION

Synthesis and characterization of nanoparticles have received considerable attention because of their use as more efficient catalysts and potential new materials (1, 2). Agglomerated silica nanoparticles in particular represent an important class of materials because of many potential applications due to their inherent thermal stability and high surface activity related to the large concentration of silanols on the surface of particles (3). Also, disperse silica (SiO_2) and alumina (Al_2O_3) are important as adsorbents and chromatographic packings (4–6). It has been shown recently that such disperse materials are essential for technological advances in photonics, quantum electronics, nonlinear optics, and information storage and processing (7–15).

The surfaces of these materials as well as of many other disperse materials used in science and technology are in general energetically heterogeneous, where the heterogeneity can be attributed to the differentiated surface and structural properties. The performance of disperse silica and alumina in various applications is highly dependent on the type of adsorption sites present on their surfaces. The active surface sites can include atoms regularly present on the surface, specific functional groups, impurities, and structural defects (16). These sites can have different magnitudes of electric charge associated with them, which is a very important factor in the interaction of the surface with polar molecules such as water.

In the current work, the surface properties of disperse silica and alumina were studied using luminescence measurements of hydrated uranyl groups under selective laser excitations. Moreover, the possibility of application of the spectroscopic characteristics of inorganic probes to the determination of the adsorption energy distribution (AED) for the disperse materials studied is shown. It has been demonstrated previously (17–20) that many ''elementary'' luminescence spectra corresponding to different types of adsorption sites contribute to the total intensity of a luminescence spectrum under integral excitation. The ''elementary'' luminescence spectra can be detected by selective laser excitation, which allows one to identify the position of the 0–0 electronic transitions on the spectrum and measure the shift of these transitions with respect to the unperturbed hydrated uranyl groups (17–20). The value of these shifts can be used for the adsorption energy evaluation for each type of adsorption site (21). In the current work particular attention has been given to the relation between the intensity distribution func-

[1] To whom correspondence should be addressed; e-mail: jaroniec@scorpio.kent.edu; Fax: 330-672-3816.

0021-9797/98 $25.00

tion of ''elementary'' spectra in the nonuniform broadened spectrum and the AED.

In addition to luminescence studies, the surface properties of silica and alumina were investigated using nitrogen adsorption and high resolution thermogravimetry (TG). Complete nitrogen adsorption–desorption isotherms were measured at −195.5°C in the relative pressure range of 10^{-6} to 0.99. The Brunauer–Emmett–Teller (BET) specific surface area S_{BET} and the total pore volume V_{t} were estimated from adsorption measurements using standard methods. Moreover, AEDs with respect to nitrogen were calculated for silica and alumina from submonolayer nitrogen adsorption data using the regularization method. These AEDs were compared with the energy distributions for water molecules of hydrated uranyl ions obtained from luminescence measurements. The TG studies were used to provide additional insight into the surface properties of the silica and alumina samples studied.

EXPERIMENTAL

(a) Sample characterization. All samples used in the luminescence studies were prepared by the following technique. Disperse silica, Aerosil (S_{BET} = 160 m^2/g; V_t = 0.58 cm^3/g) from Degussa Co. (Germany), and alumina (S_{BET} = 150 m^2/g; V_t = 0.28 cm^3/g) from the Institute of Surface Chemistry (Ukraine) were dehydrated by heating in air at 200°C for 2 h. These samples were immersed in a 2.5×10^{-3} M aqueous solution of $UO_2^{2+} \cdot 3H_2O$ at 25°C in order to cover their surfaces with hydrated UO_2^{2+} ions. Prior to the luminescence measurements the modified materials were heated in air at 27, 600, or 800°C and compacted. In the case of nitrogen adsorption measurements initial samples of disperse silica and alumina were used. Prior to analysis the silica and alumina samples were heated at 200, 600, or 800°C for 2 h in air and then degassed for 2 h at 200°C under a vacuum of about 10^{-3} Torr.

(b) Luminescence measurements. The luminescence spectra were excited by an Ar^+ laser or tunable dye laser with N_2 laser pumping. The computer-controlled laser spectrometer was used to measure the luminescence. All measurements were performed at liquid-helium temperature for dried samples. Since the luminescence response (0–0 electronic transitions) results only from the hydrated UO_2^{2+} ions, which are directly attached to the oxide surface, i.e., ions present in the monolayer, the ions present in the second and higher layers do not change this response and therefore there is no need to control strictly their concentration. Details of the method and its application have been described elsewhere (18, 21).

(c) Nitrogen adsorption measurements. Nitrogen adsorption–desorption isotherms were measured on a Micromeritics Model ASAP 2010 (Norcross, GA, USA) adsorption analyzer. The purity of nitrogen was 99.998%. Subsequently, complete nitrogen adsorption–desorption measurements at −195.5°C were measured starting in the relative pressure (p/p_0) range of approximately 10^{-6}, where p_0 denotes the saturation pressure of nitrogen vapor. The specific surface area S_{BET} was calculated using the standard BET method (22) from adsorption data in the p/p_0 range of 0.06 to 0.25. The total pore volume V_t was evaluated by converting the volume adsorbed (V in cm^3 STP/g) at p/p_0 of approximately 0.97 to the volume of liquid adsorbate.

(d) Thermogravimetric measurements. Thermogravimetric measurements were carried out using a TA Instruments Model TA 2950 (New Castle, DE, USA) thermogravimetric analyzer. Materials were heated in dry nitrogen atmosphere from ambient temperature up to 1000°C using a maximum heating rate of 5°C/min.

RESULTS

1. Adsorption Energy Distribution from Luminescence Measurements

Recently an attractive method was developed (17–20) for investigating the adsorption efficiency of disperse materials using inorganic luminescent probes (i.e., hydrated UO_2^{2+} ions) under selective laser excitation. The basic idea of this method and its application to the determination of the AEDs for heterogeneous surfaces of disperse silica and alumina are presented here.

Molecular ions experience weak perturbation resulting from interactions with the surface via the formation of adsorption complexes (ACs). The magnitude of the perturbation of molecular ions is related to the magnitude of the bonding energy in the formed AC. These weak perturbations lead to the shift of the 0–0 electronic transition and emission bands for molecular ions, which results in broad and continuous absorption and emission spectra under integral excitation. The so-called nonuniform broadening of the emission spectra that is observed is attributed to the variations in the degree of perturbation of uranyl ions under AC formation. The application of the selective laser excitation allows one to obtain many ''elementary'' luminescence spectra. For UO_2^{2+} ions the excitation wavelength was varied in the interval of approximately 480 to 520 nm, which is the 0–0 transition region for these ions. As previously stated (17–20), each ''elementary'' luminescence spectrum corresponds to a single type of AC and these ''elementary'' spectra contribute to the formation of the nonuniform broadened spectrum under integral excitation, i.e., simultaneous excitation of all types of ACs. Moreover, it has been shown (18) that there exists a correlation between the observed 0–0 electronic

transition shift and the perturbation degree of UO_2^{2+} ions for each type of AC.

The UO_2^{2+} ions are surrounded by six water molecules, arranged in the equatorial plane, and these ions interact with the silica and alumina surfaces through coordinated water molecules (17–21). The perturbation of the hydrated uranyl ions results from the interaction between water molecules coordinated to the ions and the active sites present on the silica and alumina surfaces. Therefore, an electrostatic approximation of the active surface site–water molecule interaction was considered (18–21). The value of the ''elementary'' luminescence spectrum shift is correlated with the magnitude of the electric charge on the active surface site and the adsorption energy (21). The investigation of these shifts allows one to study the surface adsorption activity and the related AED.

Generally the total integral intensity of the luminescence spectrum results from contributions of ''elementary'' luminescence spectra. This intensity can be represented as

$$S = \sum_{i=1}^{m} \int_{\nu} I_i(\nu)\mathrm{d}\nu, \qquad [1]$$

where $I_i(\nu)$ is the intensity of the electron-vibrational spectrum of the ith type of AC ($i = 1, 2, \cdots m$), which in a simple case of the interaction of the electronic transition with one vibration only (ν_1) is

$$I_i(\nu) = n_i A_i F_i(\nu), \qquad [2]$$

where

$$F_i(\nu) = \sum_{n=0}^{4} \exp\left(-\left(\frac{\nu - (\nu_{00}^{(i)} - n\nu_1^{(i)})}{\gamma^{(i)}}\right)^2\right) \times \exp(-P_\lambda^{(i)}) \frac{(P_\lambda^{(i)})^n}{n!} \qquad [3]$$

describes the spectral profile of the emission spectrum. In Eq. [2], n_i is the concentration of AC of the ith

$$A_i = \frac{1}{\tau_i} \qquad [4]$$

type in an excited state, A_i is Einstein's coefficient for a spontaneous transition, and τ_i is the time constant of the luminescence decay for the ith ''elementary'' luminescence spectrum. In Eq. [3], each electron-vibrational maximum of the ith luminescence spectrum is described by a Gaussian function and n, $\nu_{00}^{(i)}$, $\nu_1^{(i)}$, $\gamma^{(i)}$, and $P_\lambda^{(i)}$ are the vibrational quantum number, the wavenumber of the 0–0 electronic transition, the vibrational frequency in ground state, the half width of the electron-vibrational peaks, and the electron-vibrational interaction parameter, respectively. We have

$$\Phi(y) = (\phi_1, \ldots, \phi_m); \quad \phi_i = \frac{1}{S}\int_{\nu} I_i(\nu)d\nu. \qquad [5]$$

It has been shown previously (18) that the contribution of the ''elementary'' luminescence spectra can be characterized by means of the intensity distribution function as follows, where ϕ_i defines the contribution of the ith luminescence spectrum to the total integral intensity of the nonuniform broadened emission spectrum and where y is the relative shift of the ''elementary'' spectrum,

$$y = (\nu_{00}^{(0)} - \nu_{00}^{(i)})/\nu_{00}^{(0)}. \qquad [6]$$

Above $\nu_{00}^{(0)}$ is the wavenumber of the 0–0 electronic transition for the hydrated UO_2^{2+} ion unperturbed by the interactions with a surface. Because the time constant of the luminescence decay does not vary in magnitude for different ''elementary'' spectra (18), the intensity of the ith ''elementary'' spectrum is determined by the number of luminescent centers in the excited state (n_i) and is proportional to the concentration of AC of the ith type, N_i,

$$\int_{\nu} I_i(\nu)d\nu \propto n_i \propto N_i. \qquad [7]$$

Therefore, the total integral intensity is determined by the total amount of all types of ACs in the excited state (n_t) and is proportional to the total concentration of all types of ACs, N_t,

$$S \propto n_t = \sum_{i=1}^{m} n_i \propto N_t = \sum_{i=1}^{m} N_i. \qquad [8]$$

Since the excitation conditions in the case of integral and selective excitations were the same, the proportionality coefficients in Eqs. [7] and [8] can be considered equal. Then from Eqs. [5], [7], and [8] the relationship

$$\phi_i = \frac{n_i}{n_t} = \frac{N_i}{N_t} \qquad [9]$$

can be obtained, where ϕ_i now is the fraction of AC of the ith type.

Some specific intensity for each type of AC can be considered,

$$I_i^*(\nu) = \frac{1}{n_i}\int_{\nu} I_i(\nu)d\nu = A_i \int_{\nu} F_i(\nu)d\nu, \qquad [10]$$

and the total intensity can be represented in the form

$$S = \sum_{i=1}^{m} n_i I_i^*(\nu) = n_t \sum_{i=1}^{m} \phi_i I_i^*(\nu) = n_t A_i \sum_{i=1}^{m} \phi_i \int_{\nu} F_i(\nu) d\nu. \quad [11]$$

The spectral profiles of the ''elementary'' luminescence spectra have been calculated in (18) and their parameters do not differ significantly from complex to complex. Therefore, the integral in Eq. [11] can be considered constant,

$$\int_{\nu} F_i(\nu) d\nu = C, \quad [12]$$

and the following relationship is obtained:

$$S = C n_t A_i \sum_{i=1}^{m} \phi_i. \quad [13]$$

If the total number of types of ACs is large (i.e., $m \to \infty$), the sum in Eq. [13] can be replaced by an integral,

$$S = C n_t A_i \int_0^{\infty} \Phi(y) dy. \quad [14]$$

Thus, the total intensity of the luminescence spectrum is determined by the intensity distribution function $\Phi(y)$. It should be noted that ACs differ in adsorption energy only. Hence, the intensity distribution function is determined by the equilibrium distribution of the concentrations ($N(\varepsilon)$) for the different types of ACs at a specific temperature, and the concentration distribution is in turn determined by the AED. The preceding statement is correct if the energy transfer between ACs in their excited states is neglected. It has been shown previously (17–18) that the adsorption energy of the hydrated uranyl groups can be obtained by means of the value of the relative shift y for each ''elementary'' spectrum. Hence, the intensity distribution is a function of the adsorption energy ε and can be represented as (18)

$$\Phi(\varepsilon) = N(\varepsilon) \Phi^{(1)}_{\text{nonrad}}(\varepsilon) \Phi^{(2)}_{\text{nonrad}}(\varepsilon), \quad [15]$$

where $N(\varepsilon)$ is the distribution of concentrations of different types of ACs, which is invariant for samples prepared at a specific temperature, and $\Phi^{(1)}_{\text{nonrad}}(\varepsilon)$ and $\Phi^{(2)}_{\text{nonrad}}(\varepsilon)$ are functions that describe the nonradiative energy transfer resonance in highest and lowest excited states, respectively. In the subsequent discussion the luminescence spectra that were excited only in the lowest excited state will be considered. Therefore, $\Phi(\varepsilon)$ may be rewritten as,

$$\Phi(\varepsilon) = N(\varepsilon) \Phi^{(2)}_{\text{nonrad}}. \quad [16]$$

The concentration distribution for different types of ACs can be represented by using the AED,

$$N(\varepsilon) = N_t \chi^*(\varepsilon). \quad [17]$$

However, the AED function, $\chi^*(\varepsilon)$, can be obtained by taking into account the resonant energy transfer (Eq. [16]). According to (18), the resonance function $\Phi^{(2)}_{\text{nonrad}}(\varepsilon)$ is

$$\Phi^{(2)}_{\text{nonrad}}(\varepsilon) = A_n \left(\sum_{n=1}^{3} \frac{(\Gamma/2)^2}{(n\nu_1^* - \Delta\mu\epsilon - \mu_i\epsilon)^2 + (\Gamma/2)^2} + \sum_{n=1}^{10} \frac{(\Gamma/2)^2}{(n\nu_2^* - \Delta\mu\epsilon - \mu_1\epsilon)^2 + (\Gamma/2)^2} \right), \quad [18]$$

where ν_1^* and ν_2^* are the vibrational frequencies in the lowest excited state, $\Delta\mu\epsilon = \mu_2\epsilon - \mu_1\epsilon$ is the difference in the perturbation energy of the excited ($\mu_2\epsilon$) and ground ($\mu_1\epsilon$) states, μ_1 and μ_2 are the induced dipole moments of the uranyl ion in the ground and excited state, respectively, and ε is the total electric field that is created by surface charges and the induced dipole moment of water molecules at the point where the uranium atom of the uranyl ion is located. In Eq. [18], A_n and $\Gamma/2$ are the resonance intensity and the relative half width. The resonance intensities are determined by the nature of the resonant energy transfer. Because the nature of resonance for all ACs is the same (18) the intensities of ''elementary'' luminescence spectra taking into account the resonance energy transfer should be equal in magnitude for all resonance points. Hence the AED $\chi^*(\varepsilon)$ for different ACs is determined by the intensity distribution at the resonance points (see Fig. 1). In other words, the intensity distribution function $\Phi(\varepsilon)$ at the resonance points is due to the concentration distribution of different types of ACs. Therefore, Eq. [16] can be rewritten as

$$\Phi(\varepsilon) = N_t \chi^*(\varepsilon) \Phi^{(2)}_{\text{nonrad}}(\varepsilon) = N_t \chi(\varepsilon), \quad [19]$$

where $\chi(\varepsilon)$ is the real AED function taking into account the resonant energy transfer among ACs in their excited state. The AED function is normalized to unity,

$$\int_{\varepsilon_m}^{\infty} \chi(\varepsilon) d(\varepsilon) = 1, \quad [20]$$

where ε_m is the minimum adsorption energy. The function

in Eq. [20] completely defines the distribution of the ''elementary'' luminescence spectra in the integral emission spectrum, and it provides a general characterization of the energetic heterogeneity of a solid adsorbent.

It is well known (23) that the profile of the nonuniform broadened luminescence spectrum is accurately described by a Gaussian function. Therefore, for the ''elementary'' luminescence spectra (Eq. [3]) a Gaussian function was used for description of all electron-vibrational peaks because the half width of relative peaks for different uranyl salts is significantly smaller than that for the luminescence spectrum of the aqueous solution and the ''elementary'' luminescence spectra. Hence, the luminescence spectra of the uranyl salt aqueous solutions are evenly nonuniform broadened and may be described by a Gaussian function. Moreover, the total intensity of the nonuniform broadened spectrum under integral excitation, where all spectral components of the broadening are the ''elementary'' luminescence spectra, can also be described by a Gaussian distribution. Therefore, one can consider the Gaussian distribution of the adsorption energy,

$$\chi(\varepsilon) = C_n \exp\left(-\left(\frac{\varepsilon_n - \varepsilon_n^{(m)}}{\gamma_n}\right)^2\right), \qquad [21]$$

where $\varepsilon_n^{(m)}$ is the ''elementary'' spectrum which contributes the most to the AED, γ_n describes the spread of the distribution, and C_n is a normalization constant which depends on the limits of integration. Shown in Fig. 2 are the AED functions for silica and alumina, which have been calculated from the adsorption energies of different types of ACs (21) using Eq. [19]. The AED for the silica sample prepared at 300 K can be characterized by two peaks which correspond

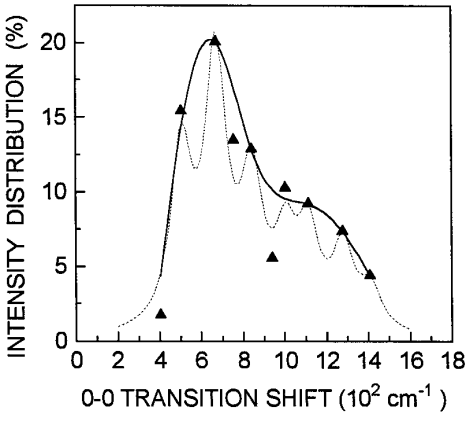

FIG. 1. The intensity distribution function of the contributions for elementary spectra versus the 0–0 electronic transition shifts. Points represent experimental results, which were obtained by integrating intensities of elementary spectra; the solid line represents a spline of resonance points, the dashed line represents a resonance energy transfer function.

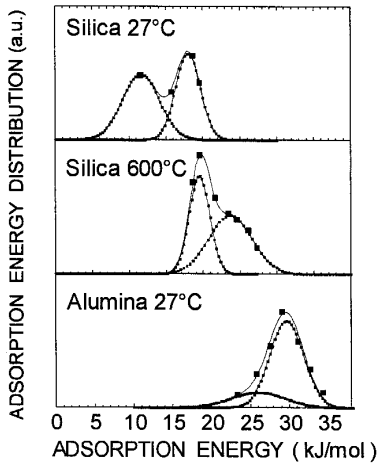

FIG. 2. The AED functions obtained from luminescence measurements of hydrated uranyl groups for the disperse silica and alumina. The dashed lines represent Gaussian components of the AEDs. The solid lines are the sum of different Gaussian components.

to the physical and chemical adsorption, respectively. The dashed lines in Fig. 2 represent the approximate AEDs obtained using the Gaussian function (Eq. [21]). The parameters of the Gaussian function are listed in Table 1.

According to IR measurements (24), at 27°C the silica surface is hydrated and hydroxylated, whereas the sample prepared at 600°C is dehydrated but not dehydroxylated. It can be assumed that ACs formed at 27°C interact only via hydrogen bonding. This assumption is realistic because the surface is hydrated and all active sites are blocked by water molecules. Therefore, the first peak in the AED can be assigned to physical adsorption of water molecules of hydrated uranyl groups. In the case of the dehydrated surface (the silica sample prepared at 600°C) the aforementioned peak disappears, and the second peak is shifted insignificantly in the direction of higher energies and corresponds to the chemical adsorption of water molecules coordinated in the hydrated uranyl group. It should be noted that this peak for the silica sample prepared at 600°C is characterized by a shoulder at higher values of the adsorption energy. The AED for the alumina sample prepared at 27°C can be also characterized by a shoulder, but it is located at lower values of the adsorption energy.

2. Adsorption Energy Distribution from Nitrogen Adsorption

AED functions for silica and alumina were calculated from submonolayer adsorption data (i.e., $V < V^0$, where V and V^0 denote the volume adsorbed and the BET monolayer capacity, respectively) by inverting the integral equation of adsorption (5, 6, 25),

$$\Theta(p) = \int_{\varepsilon_{\min}}^{\varepsilon_{\max}} \theta(p, \varepsilon)\chi(\varepsilon)d\varepsilon, \qquad [22]$$

TABLE 1
Gaussian Parameters for Different Maxima (n) on AEDs Obtained from Luminescence Measurements of Hydrated Uranyl Groups for the Disperse Silica and Alumina Samples

	Silica						Alumina		
	$T_{h.t.}$ = 27°C			$T_{h.t.}$ = 600°C			$T_{h.t.}$ = 27°C		
n	C_n	$\epsilon_n^{(m)}$ (kJ/mol)	γ_n (kJ/mol)	C_n	$\epsilon_n^{(m)}$ (kJ/mol)	γ_n (kJ/mol)	C_n	$\epsilon_n^{(m)}$ (kJ/mol)	γ_n (kJ/mol)
1	1.08	1.16	5.0	1.97	19.51	2.75	0.4	26.0	7.0
2	1.24	18.0	3.33	0.99	23.68	5.84	1.41	29.69	4.35

where $\Theta(p)$ is the total adsorption isotherm in the submonolayer range defined as the ratio of the amount adsorbed to the BET monolayer capacity, p is the equilibrium pressure, ε is the adsorption energy, $\theta(p, \varepsilon)$ is the local adsorption isotherm as a function of the adsorption energy, and $\chi(\varepsilon)d\varepsilon$ is the fraction of the surface with adsorption energies between ε and $\varepsilon + d\varepsilon$. The local adsorption isotherm $\theta(p, \varepsilon)$ was represented by the Fowler–Guggenheim (FG) (26) equation, which describes localized monolayer adsorption with lateral interactions on an energetically homogeneous surface,

$$\theta(p, \varepsilon) = \frac{Kp \exp(z\omega\Theta/k_BT)}{1 + Kp \exp(z\omega\Theta/k_BT)}, \qquad [23]$$

where K is the Langmuir constant for adsorption on monoenergetic sites, z is the number of nearest neighbors to an adsorbate molecule in the monolayer, ω is the interaction energy between nearest neighbors, and k_B and T have their usual meanings. The Langmuir constant K is defined as

$$K = K_0(T)\exp(\varepsilon/k_BT), \qquad [24]$$

where $K_0(T)$ is the preexponential factor expressed in terms of the partition functions for an isolated molecule in the gas and surface phases (27). The form of the FG equation presented above implies a random distribution of adsorption sites (as opposed to a patchwise distribution), which seems to be a realistic model for the surfaces of amorphous inorganic oxides such as silica and alumina (6, 28). The AEDs for silica and alumina were calculated using the INTEG program available in the laboratory, which employs the regularization method (29) to invert the integral equation of adsorption with respect to $\chi(\varepsilon)$. The interaction parameters $z = 4$, $\omega/k_BT = 1.23$, and the regularization parameter $\gamma = 0.01$ were assumed in the calculations. The AED functions for silica and alumina resulting from nitrogen adsorption were calculated for samples prepared at 200, 600, and 800°C and are shown in Figs. 3 and 4, respectively. There are three contributions to the AED functions, which were described by using Gaussian profiles. The parameters of the Gaussian function are listed in Table 2.

3. Thermogravimetric Measurements

Let us consider the water removing process by using thermogravimetric measurements. Thermogravimetric curves for silica samples measured in nitrogen and air atmosphere are shown in Fig. 5a, curves 1, 2. The general view of the TG curves practically does not change when air is flowing instead of nitrogen, except the region between 800 and 1000°C. In this high-temperature region a small difference can be observed, as shown in Fig. 5b. In addition, the dependence of the integral optical density of the IR absorption band at 3748 cm^{-1}, which corresponds to stretching vibrations of free surface hydroxyls, on the pretreatment temperature of the samples is shown in Fig. 5a, curve 3 (24). A drastic decrease in the sample weight can be observed in the temper-

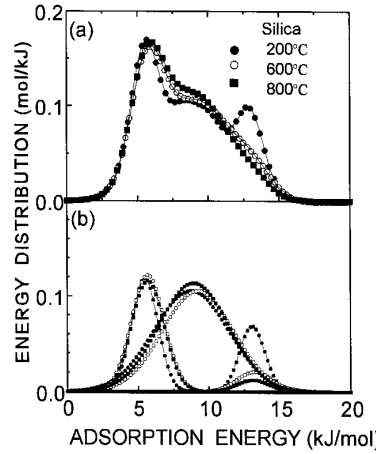

FIG. 3. (a) The AED function obtained from nitrogen adsorption measurements for the disperse silica. (b) The corresponding Gaussian components of the AED.

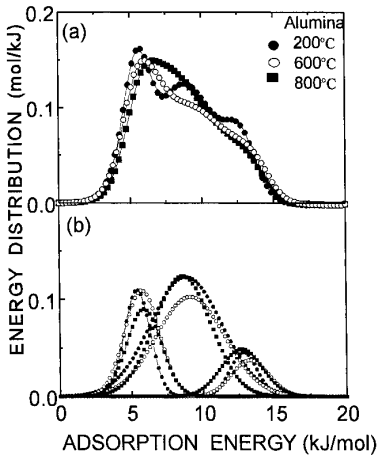

FIG. 4. (a) The AED function obtained from nitrogen adsorption measurements for the disperse alumina. (b) The corresponding Gaussian components of the AED.

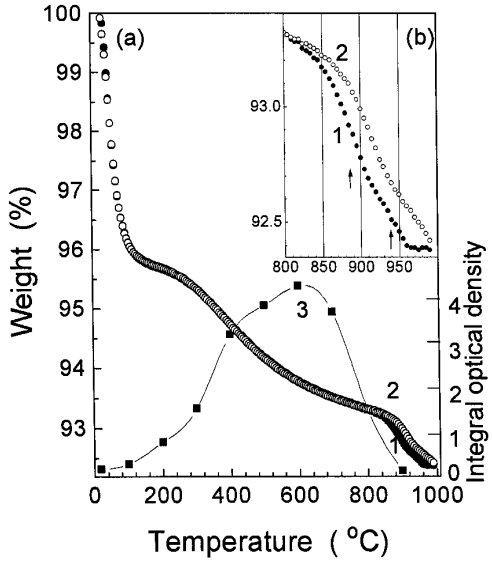

FIG. 5. The thermogravimetric weight-change curves for the disperse silica (a) and their high-temperature segments (b) measured in nitrogen (1) and air (2) atmosphere. The dependence of the integral optical density of the IR absorption band at 3748 cm^{-1} on the pretreatment temperature of the samples is also shown (3) [24]. The thermogravimetric curves were normalized. The differences in the weight loss for different runs were ~0.5%. Arrows indicate two stages of the crystalline quartz phase formation.

ature region 30–120°C and is attributed to the desorption of physically adsorbed water molecules. The next stage of weight loss is caused by two processes. The first is the removal of bonded water molecules from the oxide surface and the second is related to the condensation and removal of surface silanol groups. These conclusions are supported by using IR measurements (Fig. 5a, curve 3). The temperature region where the concentration of free silanol groups increases corresponds to the removal of the bonded water molecules because active sites for these molecules are the silicon atoms of silanol groups (16). A decrease in concentration of free surface silanol groups corresponds to their condensation and removal with nonbridging oxygen atoms (NBOA) and peroxy linkage formation. These processes can be represented as (30)

$$2\ (\equiv\mathrm{Si}-\mathrm{OH}) \xrightarrow{T_{\mathrm{h.t.}}>600^{\circ}\mathrm{C}} (\equiv\mathrm{Si}-\mathrm{O}\cdot) + \equiv\mathrm{Si}\cdot + \mathrm{H_2O} \quad [25]$$

$$2\ (\equiv\mathrm{Si}-\mathrm{OH}) \xrightarrow{T_{\mathrm{h.t.}}>600^{\circ}\mathrm{C}} (\equiv\mathrm{Si}-\mathrm{O}-\mathrm{O}-\mathrm{Si}\equiv) + \mathrm{H_2}, \quad [26]$$

where "≡" denotes the three bonds and "·" represents

TABLE 2
Gaussian Parameters for Different Maxima (n) on AEDs Obtained from Nitrogen Adsorption Measurements for the Disperse Silica and Alumina Samples

	$T_{\mathrm{h.t.}}$ = 200°C			$T_{\mathrm{h.t.}}$ = 600°C			$T_{\mathrm{h.t.}}$ = 800°C		
n	C_n	$\epsilon_n^{(m)}$ (kJ/mol)	γ_n (kJ/mol)	C_n	$\epsilon_n^{(m)}$ (kJ/mol)	γ_n (kJ/mol)	C_n	$\epsilon_n^{(m)}$ (kJ/mol)	γ_n (kJ/mol)
					Silica				
1	0.119	5.46	1.32	0.122	5.67	1.66	0.116	5.67	1.62
2	0.105	8.75	3.75	0.105	9.21	3.54	0.114	8.93	3.51
3	0.068	13.05	1.27	0.021	13.22	1.76	0.012	13.09	1.64
					Alumina				
1	0.110	5.40	1.29	0.109	5.72	1.74	0.090	5.86	1.72
2	0.123	8.88	3.54	0.103	9.11	3.40	0.124	8.57	2.80
3	0.045	12.80	1.35	0.038	13.26	1.85	0.049	12.67	2.06

the unpaired spin. Some of the supporting evidence for such a process was obtained by measuring characteristic red luminescence of NBOAs (7, 31) and the observation of the Raman peak at 610 cm^{-1} related to peroxy linkage formation (12). It was stated in the Raman spectra study that the formation of the crystalline structure occurs at $T_{h.t.} \sim 1000°C$ (12). This process also causes a drastic increase in the efficiency of the second harmonic generation in the collection of silica nanoparticles, which is due to the nonlinear property of the crystalline quartz phase (32). It can be assumed that this process is reflected in the last stage in weight loss on the TG curve and can be represented by the reactions

$$(\equiv Si—O\cdot) + \equiv Si\cdot \xrightarrow{T_{h.t.}>900°C} \equiv(\equiv Si—O—Si\equiv) \quad [27]$$

$$(\equiv Si—O—O—Si\equiv) \xrightarrow{T_{h.t.}>900°C}$$

$$\equiv Si\cdot + (\cdot O—O—Si\equiv) \quad [28]$$

$$(\equiv Si——O—O\cdot) + \equiv(Si—O\cdot) \xrightarrow{T_{h.t.}>900°C}$$

$$(\equiv Si—O—Si\equiv) + O_2. \quad [29]$$

The last process is oxygen-dependent and therefore must be retarded in the presence of molecular oxygen during heat treatment at high temperatures. It is well known that the release of oxygen from different types of vitreous silica occurs in a molecular form (33, 34). Hence, the difference in TG curves in the temperature region 800–1000°C can be explained by the presence of molecular oxygen in an air atmosphere. Note that the disappearance of the Raman peak at 610 cm^{-1} for the sample which was heat pretreated at 1000°C (12) supports the correctness of reactions [28] and [29]. It should be noted also that there are two stages of crystalline structure formation during the heat pretreatment in nitrogen atmosphere. These stages are marked by arrows in Fig. 5b and shown in Fig. 6 on the differential TG curve. In a previous study (12) it was suggested that the collection of small silica particles possesses two media of different dielectric constants. Therefore, two stages of the crystalline structure formation offer direct evidence for the presence of two aggregates of small silica particles. These stages are shifted to the higher temperature region when silica samples are heated in air (see Fig. 6).

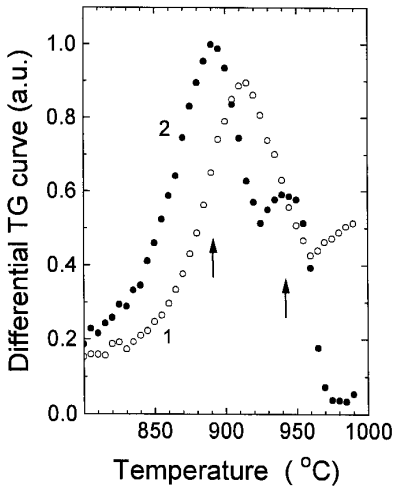

FIG. 6. The part of the differential TG curve for the disperse silica measured in nitrogen (1) and air (2) atmosphere. Arrows indicate two stages of crystalline quartz phase formation.

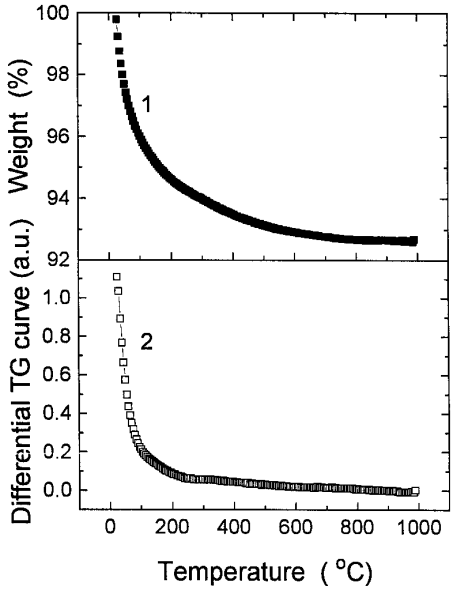

FIG. 7. The TG curve (1) and its derivative (2) of the disperse alumina measured in nitrogen atmosphere.

The TG curve for the alumina sample measured in nitrogen and air atmospheres practically coincide, as shown in Fig. 7. Experimental conditions in this case give no way of indicating the stages of the weight loss.

DISCUSSION

As has been shown in the preceding section, a bimodal AED is observed for initial samples of disperse silica and alumina in the case of water adsorption. Since the low-energy peak for disperse silica disappears during heat treatment up to 600°C it can be attributed to the physically adsorbed water molecules of the hydrated uranyl groups which interact with the surface silanols. This conclusion is in good agreement with the IR measurements of the heat treatment dynamics of disperse silica (24). Accordingly, the high-energy peak is assigned to the chemically adsorbed water molecules. On the other hand, heat treatment of the silica

samples causes some transformation of the high-energy peak to a broad shoulder in the range of high energies, which also indicates a bimodal character of the AED in the case of chemical adsorption. For the initial alumina sample the shoulder is located in the low energy range and the AED is shifted to the high-energy range because the charge values on the surface hydroxyls are higher in the case of disperse alumina than in the case of the silica surface (18, 20). It should be noted that in the adsorption energy evaluation the electrostatic approximation was used because the amount of charge transfer between the active site and the water molecules is quite small, and the interaction is basically caused by the Coulombic electrostatic interaction between the surface charge and the dipole moment of water molecules (35–38).

Evidently, the peak positions on AEDs evaluated from water and nitrogen adsorptions are different, indicating a different nature of adsorption interactions between molecules and the surface. As was mentioned above, water molecules are characterized by a dipole moment, and the basic contribution to the adsorption energy arises from electrostatic interactions. In contrast, nitrogen molecules are nonpolar and interactions with the surface are caused by weaker van der Waals type interactions. Peaks on the AEDs can be fitted by Gauss profiles, and some changes in the shape of distributions can be explained by varying contributions corresponding to the different peaks. As can be seen from Table 2, the peak positions practically do not change for silica and alumina samples prepared at different temperatures, and all changes in the shape of AEDs result from the changes in the fraction of the different types of active sites on the disperse materials' surface. The peak at 13.1–13.2 kJ/mol in the case of the disperse silica, which is drastically decreased by the heat treatment up to 600°C, can be attributed to nitrogen adsorption on water molecules linked to the surface. A further decrease in this peak for samples treated up to 800°C results from the condensation of silanols and their removal from the surface. These facts are supported by thermogravimetric measurements (Fig. 5). This peak does not decrease significantly in the case of alumina samples. It appears that this results from the higher thermal stability of surface OH groups on disperse alumina (39) and the condensation in this case occurs at a higher temperature in comparison to that on the silica surface.

Two peaks on the AED, located at 5.4–5.8 and 8.7–9.2 kJ/mol, are caused by nitrogen adsorption on two other different types of surface active sites. These two types of active sites on silica and alumina surfaces are present on the AED for samples prepared at different temperatures and practically do not change during heat treatment. In the case of disperse alumina the peak at 5.4–5.8 kJ/mol decreases during heat treatment of this sample from 600 to 800°C, resulting in the change of the AED shape. Another peak at 8.75–9.11 kJ/mol decreases insignificantly during heating of the sample from 200 to 600°C and then moves back during heating from 600 to 800°C. A basic question is: What is the nature of two peaks of AED, neglecting the peak that is related to water molecules linked to the surface? These two peaks are present on the AEDs obtained from both nitrogen adsorption and luminescence measurements for the silica and alumina samples. Moreover, such a bimodal distribution was also measured by using adsorption of different gases on the silica surface: hexane, heptane, octane (40), hexane, hexene, pentane, pentene (41), butane, and butene (42). It would be desirable in the future to use these experimental results for theoretical considerations of this problem.

Finally, we can conclude that the luminescence method of the AED evaluation presented in the current work can be useful for characterization of different disperse materials having heterogeneous surfaces.

ACKNOWLEDGMENT

Partial support of this work by the American National Research Council is acknowledged.

REFERENCES

1. Siegel, R. W., *Annu. Rev. Mater.Sci.* **21,** 559 (1991); *Nanostruct. Mater.* **4,** 121 (1994).
2. Pool, R., *Science* **248,** 1186 (1990).
3. Che, M., and Bennett, C. O., *Adv. Catal.* **36,** 55 (1989).
4. Jaroniec, M., and Madey, R., ''Physical Adsorption on Heterogeneous Solids.'' Elsevier, Amsterdam, 1988.
5. Rudzinski, W., and Everett, D., ''Adsorption of Gases on Heterogeneous Surfaces.'' Academic Press, London, 1992.
6. Jaroniec, M., *in* ''Adsorption on New and Modified Inorganic Adsorbents'' (A. Dabrowski and V. A. Tertykh, Eds.), p. 411. Elsevier, Amsterdam, 1996.
7. Glinka, Yu. D., Degoda, V. Ya., and Naumenko, S. N., *J. Non-Cryst. Solids* **152,** 219 (1993).
8. Glinka, Yu. D., *Appl. Phys. Lett.* **70,** 1336 (1997).
9. Glinka, Yu. D., *Zh. Eksp. Teor. Fiz.* **111,** 1748 (1997); *JETP Lett. (Eng Transl)* **84,** 957 (1997).
10. Glinka, Yu. D., *Appl. Phys. Lett.* **71,** 566 (1997).
11. Glinka, Yu. D., and Jaroniec, M., *Phys. Rev. A* **56,** 3056 (1997).
12. Glinka, Yu. D., and Jaroniec, M., *J. Appl. Phys.* **82,** 3499 (1997).
13. Glinka, Yu. D., and Jaroniec, M., *J. Phys. Chem. B.* **101,** 8832 (1997).
14. El-Shall, M. S., Li, S., Turkki, T., Graver, D., Pernisz, U. C., and Daraton, M. I., *J. Phys. Chem.* **99,** 17805 (1995).
15. Li, S., Silvers, S. J., and El-Shall, M. S., *J. Phys. Chem.* **101,** 1794 (1997).
16. Gorlov, Yu. I., and Chuiko, A. A., ''Surface Chemistry of Silica: Surface Structure, Active Centers, Sorption Mechanisms.'' Naukova Dumka, Kiev, 1992. [in Russian]
17. Glinka, Yu. D., Krak, T. B., and Belyak, Yu. N., *J. Mol. Struct.* **349,** 215 (1995).
18. Glinka, Yu. D., and Krak, T. B., *Phys. Rev. B* **52,** 14985 (1995).
19. Glinka, Yu. D., Krak, T. B., Belyak, Yu. N., Degoda, V. Ya., and Ogenko, V. M., *Colloids Surfaces A* **104,** 17 (1995).
20. Glinka, Yu. D., and Krak, T. B., *Fresenius Z. Anal. Chem.* **355,** 647 (1996).

21. Glinka, Yu. D., Jaroniec, M., and Rozenbaum, V. M., *J. Colloids Interface Sci.* **194,** 455 (1997).
22. Sing, K. S. W., Everett, D. H., Haul, R. A. W., Moscou, L., Pierotti, R. A., Rouquerol, J., and Siemieniewska, T., *Pure Appl. Chem.* **57,** 603 (1985).
23. Demtröder, W., ''Laser Spectroscopy (Basic Concepts and Instrumentation).'' Springer-Verlag, Berlin/New York, 1982.
24. Belyak, Yu. N., Glinka, Yu. D., Krut', A. V., Naumenko, S. N., Ogenko, V. M., and Chuiko, A. A., *Zh. Prikl. Spektrosk.* **59,** 77 (1993); *J. Appl. Spectr.* **59,** 515 (1993).
25. Jaroniec, M., and Brauer, P., *Surface Sci. Rep.* **6,** 65 (1986).
26. Fowler, R. H., and Guggenheim, E. A., ''Statistical Thermodynamics.'' Cambridge Univ. Press, London, 1949.
27. Clark, A., ''The Theory of Adsorption and Catalysis.'' Academic Press, New York, 1970.
28. Jaroniec, M., *Adv. Colloid Interface Sci.* **18,** 149 (1983).
29. Von Szombathely, M., Brauer, P., and Jaroniec, M., *J. Comput. Chem.* **13,** 17 (1992).
30. Moulson, A. J., and Roberts, J. P., *J. Chem. Soc. Faraday Trans.* **57,** 1208 (1961).
31. Glinka, Yu. D., Naumenko, S. N., Ogenko, V. M., and Chuiko, A. A., *Opt. Spektrosk.* **71,** 431 (1991) [*Opt. Spectrosc. (USSR)* **71,** 250 (1991)].
32. Glinka, Yu. D., Krak, T. B., and Naumenko, S. N., *in* ''Fundamentals of Adsorption: Proc. 5th Int. Conf. on Fundamentals of Adsorption'' (M. D. LeVan, Ed.). p. 313. Kluwer Academic, Boston, 1996.
33. Morimoto, Yu., Igarashi, I., Sagahara, H., and Nasu, S., *J. Non-Cryst. Solids* **139,** 35 (1992).
34. Williams, E. L., *J. Am. Ceram. Soc.* **48,** 190 (1965).
35. Clementi, E., and Popkie, H., *J. Chem. Phys.* **57,** 1077 (1972).
36. Kistenmacher, H., Popkie, H., and Clementi, E., *J. Chem. Phys.* **58,** 1689 (1973).
37. Kistenmacher, H., Popkie, H., and Clementi, E., *J. Chem. Phys.* **58,** 5627 (1973).
38. Kistenmacher, H., Popkie, H., and Clementi, E., *J. Chem. Phys.* **59,** 5842 (1973).
39. Peri, J. B., *J. Phys. Chem.* **69,** 211 (1965).
40. Jagiello, J., Ligner, G., and Papirer, E., *J. Colloid Interface Sci.* **137,** 128 (1990).
41. Tijburg, I., Jagiello, J., Vidal, A., and Papirer, E., *Langmuir* **7,** 2243 (1991).
42. Jagiello, J., Bandosz, T. J., Putyera, K., and Schwarz, J. A., *in* ''Fundamentals of Adsorption: Proc. 5th Int. Conf. on Fundamentals of Adsorption'' (M. D. LeVan, Ed.). p. 417. Kluwer Academic, Boston, 1996.